TRPV4 channels stimulate Ca^{2+}-induced Ca^{2+} release in astrocytic endfeet and amplify neurovascular coupling responses

Kathryn M. Dunn[a], David C. Hill-Eubanks[a], Wolfgang B. Liedtke[b], and Mark T. Nelson[a,c,1]

[a]Department of Pharmacology, University of Vermont, Burlington, VT 05405; [b]Department of Medicine and Neurobiology and Center for Translational Neuroscience, Duke University Medical Center, Durham, NC 27710; and [c]Institute of Cardiovascular Sciences, University of Manchester, Manchester M13 9NT, United Kingdom

Edited by Michael D. Cahalan, University of California, Irvine, CA, and approved February 25, 2013 (received for review September 21, 2012)

In the CNS, astrocytes are sensory and regulatory hubs that play important roles in cerebral homeostatic processes, including matching local cerebral blood flow to neuronal metabolism (neurovascular coupling). These cells possess a highly branched network of processes that project from the soma to neuronal synapses as well as to arterioles and capillaries, where they terminate in "endfeet" that encase the blood vessels. Ca^{2+} signaling within the endfoot mediates neurovascular coupling; thus, these functional microdomains control vascular tone and local perfusion in the brain. Transient receptor potential vanilloid 4 (TRPV4) channels—nonselective cation channels with considerable Ca^{2+} conductance—have been identified in astrocytes, but their function is largely unknown. We sought to characterize the influence of TRPV4 channels on Ca^{2+} dynamics in the astrocytic endfoot microdomain and assess their role in neurovascular coupling. We identified local TRPV4-mediated Ca^{2+} oscillations in endfeet and further found that TRPV4 Ca^{2+} signals are amplified and propagated by Ca^{2+}-induced Ca^{2+} release from inositol trisphosphate receptors (IP_3Rs). Moreover, TRPV4-mediated Ca^{2+} influx contributes to the endfoot Ca^{2+} response to neuronal activation, enhancing the accompanying vasodilation. Our results identify a dynamic synergy between TRPV4 channels and IP_3Rs in astrocyte endfeet and demonstrate that TRPV4 channels are engaged in and contribute to neurovascular coupling.

calcium | parenchymal arteriole

Astrocytes are glial cells in the brain that are essential for the structural and functional integrity of the central nervous system. Astrocytes maintain cerebral homeostasis by acting as "switchboards," receiving and integrating communication from the surrounding microenvironment and translating that information into physiological and homeostatic responses. Numerous astrocytic projections make contact with neighboring synapses, while other projections terminate in "endfeet" that spread out and wrap around parenchymal arterioles and capillaries within the brain (1, 2). This structural orientation allows astrocytes to monitor synaptic activity in neuronal networks and mediate communication between neurons and the cerebral microcirculation.

Calcium (Ca^{2+}) signaling is critical for astrocyte function. Transient increases in intracellular Ca^{2+} concentration ($[Ca^{2+}]_i$) mediated by inositol 1,4,5-trisphosphate (IP_3) receptor Ca^{2+} release channels (IP_3Rs) in endoplasmic reticulum (ER) membranes drive the release of chemical transmitters like glutamate, adenosine triphosphate (ATP), and D-Serine that modulate synaptic transmission and neuronal excitability (3, 4). IP_3R-dependent Ca^{2+} signaling in astrocytes is also critical for neurovascular coupling (NVC), the process by which local cerebral blood flow (CBF) is matched to neuronal metabolism (5, 6). As neuronal activity increases, synaptically released glutamate binds to metabotropic glutamate receptors (mGluRs) on perisynaptic astrocytic projections, stimulating phospholipase C-dependent IP_3 release from membrane phospholipids. Liberated IP_3 initiates an IP_3R-dependent Ca^{2+} signal that propagates as a wave from perisynaptic processes through the astrocyte to the perivascular endfoot (7). When the IP_3R-dependent Ca^{2+} wave reaches the endfoot, the rise in endfoot $[Ca^{2+}]_i$ activates Ca^{2+}-sensitive pathways to release vasoactive substances that cause the adjacent arteriole to dilate (8, 9). Endfoot $[Ca^{2+}]_i$ is thus coupled to vascular diameter and local perfusion, but there is a duality to this relationship: moderate increases in endfoot $[Ca^{2+}]_i$ dilate parenchymal arterioles, whereas high endfoot $[Ca^{2+}]_i$ constricts them (10). This bidirectional vascular response means that endfoot Ca^{2+} must be finely regulated to ensure adequate perfusion and maintain cerebral homeostasis.

The astrocytic endfoot is therefore a specialized Ca^{2+} signaling domain, acting as a vasoregulatory unit, and IP_3Rs play a significant role in endfoot Ca^{2+} signaling (6). The contribution of other pathways to astrocytic endfoot Ca^{2+} signaling and the dynamic regulation of these pathways are not well characterized. However, immunofluorescence and immunogold electron microscopy evidence suggests that TRPV4 channels—plasma membrane cation channels of the transient receptor potential vanilloid (TRPV) family—are localized in astrocytic endfeet; moreover, 4α-phorbol 12,13-didecanoate (4αPDD), a TRPV4-selective chemical activator, increases $[Ca^{2+}]_i$ in cultured cortical astrocytes (11). Also in cultured cortical astrocytes, TRPV4 channels form complexes with aquaporin 4 to regulate cell volume responses to hypoosmotic stress (12). Notably, it has been shown that TRPV4 channels in other preparations are activated by epoxyeicosatrienoic acids (EETs) (13–15), which have been implicated in NVC (16–18) and reportedly stimulate Ca^{2+} influx in rat cortical astrocytes (19, 20). TRPV4 channels are thermosensitive, osmosensitive, and mechanosensitive, and thereby mediate processes by which cells sense and respond to environmental cues (21–24). Like IP_3Rs, TRPV4 channel activity is potentiated by modest elevations of $[Ca^{2+}]_i$ and inhibited by high $[Ca^{2+}]_i$ (25–29). Endfoot TRPV4 channel activity could, therefore, have a broad impact on astrocytic sensory and vasoregulatory functions. However, TRPV4 Ca^{2+} signaling has not been characterized in native astrocytic endfeet.

We hypothesized that the Ca^{2+}-permeable TRPV4 channel constitutes a Ca^{2+}-signaling module in the endfoot microdomain. Here, we provide functional evidence for TRPV4 channels in perivascular astrocytic endfeet and demonstrate a dynamic synergy between TRPV4-mediated Ca^{2+} entry and ER Ca^{2+} release through IP_3Rs. Our results also indicate that TRPV4-mediated Ca^{2+} entry plays a role in astrocytic endfoot regulation of the

Author contributions: K.M.D. and M.T.N. designed research; K.M.D. performed research; W.B.L. contributed new reagents/analytic tools; K.M.D. analyzed data; and K.M.D., D.C.H.-E., and M.T.N. wrote the paper.

The authors declare no conflict of interest.

This article is a PNAS Direct Submission.

[1]To whom correspondence should be addressed. E-mail: Mark.Nelson@uvm.edu.

This article contains supporting information online at www.pnas.org/lookup/suppl/doi:10.1073/pnas.1216514110/-/DCSupplemental.

NEUROSCIENCE

cerebral microcirculation and contributes to the endfoot Ca^{2+} response to neuronal activity. These results suggest a model in which Ca^{2+} entry and release mechanisms interact to sculpt astrocyte Ca^{2+} dynamics and thus fine tune astrocytic endfoot function.

Results

TRPV4 Channel Activation Increases Endfoot Ca^{2+} Signaling. Multiphoton fluorescence imaging with simultaneous infrared light–differential interference contrast (IR-DIC) microscopy enabled visualization of cortical parenchymal arterioles in coronal brain slices from adult mice, including the arteriolar lumen with red blood cells, smooth muscle cells (SMCs), and surrounding astrocytic endfeet loaded with the fluorescent Ca^{2+}-binding dye, Fluo-4 AM (field of view = 62 × 62 μm) (Fig. 1*A*).

Traces in Fig. 1 (*C*, *a*; *D*, *a*; and *E*, *a*) show changes in fractional fluorescence ($\Delta F/F_o$) of Fluo-4 AM in 1-μm^2 regions of interest (ROIs) on astrocytic endfeet, indicating endfoot Ca^{2+} levels. We assigned the threshold for a Ca^{2+} event, or "oscillation," as 0.3 $\Delta F/F_o$, which is ~2 SDs above the mean fluorescence fluctuation. Ca^{2+} oscillations, a general term used here to refer to any transient increase in endfoot Ca^{2+} that exceeds the 0.3 $\Delta F/F_o$ threshold, occurred spontaneously at low frequency (~1/min) in unstimulated astrocytic endfeet and were primarily in the form of propagating Ca^{2+} waves (nondecremental, propagating Ca^{2+} oscillations that traveled a distance >10 μm) as opposed to localized oscillations. An example of a spontaneous Ca^{2+} oscillation is evident in the baseline recording period in the trace in Fig. 1*D*, *a*. Exposure of brain slices to the selective TRPV4 agonist, GSK1016790A (hereafter GSK; 100 nM) (30), induced rapid, high-amplitude Ca^{2+} oscillations in endfeet, increasing oscillation frequency by 417% ± 113% (Fig. 1*C*, *b*). GSK increased the maximum amplitude of Ca^{2+} oscillations by 77% ± 19%, from 0.32 ± 0.07 $\Delta F/F_o$ to 1.34 ± 0.25 $\Delta F/F_o$ (n = 7 slices from six animals) (Fig. 1*C*, *c* and Movie S1). It should be noted that an increase in oscillation amplitude could move subthreshold events that were "missed" during baseline recording above the threshold, thereby contributing to the apparent increase in frequency. The endfoot Ca^{2+} oscillations elicited by GSK were mostly Ca^{2+} waves (Fig. 1*B* and Fig. S1). GSK had no effect on endfoot Ca^{2+} activity in TRPV4$^{-/-}$ mice (n = 4 slices from two animals) (Fig. 1*D*), or in slices preincubated with the selective TRPV4 antagonist, HC-067047 (10 μM; n = 6 slices from four animals) (Fig. 1*E*) (31). Whereas the increase in endfoot Ca^{2+} oscillations to GSK was prevented by HC-067047, there was no apparent effect of HC-067047 on spontaneous endfoot Ca^{2+} oscillation frequency (Control, n = 16; HC, n = 9) (Fig. S2*A*), suggesting that these spontaneous oscillations are not dependent on TRPV4 channel activity.

We found that, like GSK, 11,12-EET (1 μM), a proposed endogenous activator of TRPV4 channels, induced rapid, high-amplitude Ca^{2+} oscillations, increasing amplitude by 52% ± 13%, from 0.75 ± 0.13 $\Delta F/F_o$ to 1.66 ± 0.22 $\Delta F/F_o$ (n = 4 slices from three animals) (Fig. 2*B*, *c* and Movie S2). This effect of 11,12-EET on endfoot Ca^{2+} was blocked by HC-067047 (Fig. 2*C*), suggesting a TRPV4 channel-mediated effect. We found that 11,12-EET did not significantly increase oscillation frequency (Fig. 2*B*, *b*). Collectively, these results support the existence of functional TRPV4 channels in perivascular astrocytic endfeet and provide evidence that EETs are capable of activating these channels to increase astrocytic endfoot Ca^{2+} signaling.

Ca^{2+} Entry Through TRPV4 Channels Stimulates IP_3R-Mediated Ca^{2+} Release in Astrocytic Endfeet. IP_3Rs in ER membranes are activated by Ca^{2+} and mediate Ca^{2+} waves. Accordingly, we hypothesized that ER Ca^{2+} release contributes to the endfoot Ca^{2+} oscillations elicited by TRPV4 channel activation. To minimize ER Ca^{2+} release, we depleted ER Ca^{2+} stores by inhibiting ER Ca^{2+} reuptake using the sarcoplasmic reticulum (SR)/ER Ca^{2+} ATPase (SERCA) inhibitor, cyclopiazonic acid (CPA; 30 μM) (6). CPA nearly eliminated spontaneous endfoot Ca^{2+} activity (Fig. S2*B*). After incubation with CPA, GSK still stimulated endfoot Ca^{2+} signaling, increasing the frequency (Fig. 3*B*, *b*) and amplitude (Fig. 3*B*, *c*) of Ca^{2+} oscillations. However, as is evident in Fig. 3*A* and the trace in Fig. 3*B*, *a*, the spatiotemporal characteristics of Ca^{2+} oscillations induced by GSK were markedly different in the presence of CPA (Movie S3). With CPA present, GSK-induced endfoot Ca^{2+} oscillations were slow, low-amplitude (0.75 ± 0.05 $\Delta F/F_o$; Fig. 3*B*, *c*), localized events. In the example depicted in Fig. 3*A*, the duration of the Ca^{2+} oscillation was 37.1 s. These oscillations had a spatial spread of 9 ± 1 μm (n = 9), compared with the propagating Ca^{2+} oscillations seen with GSK under normal conditions, which had a spatial spread of 27 ± 2 μm (n = 27; Fig. 3*C*). Moreover, local increases in endfoot Ca^{2+} were lower amplitude and exhibited slower on/off kinetics after treatment

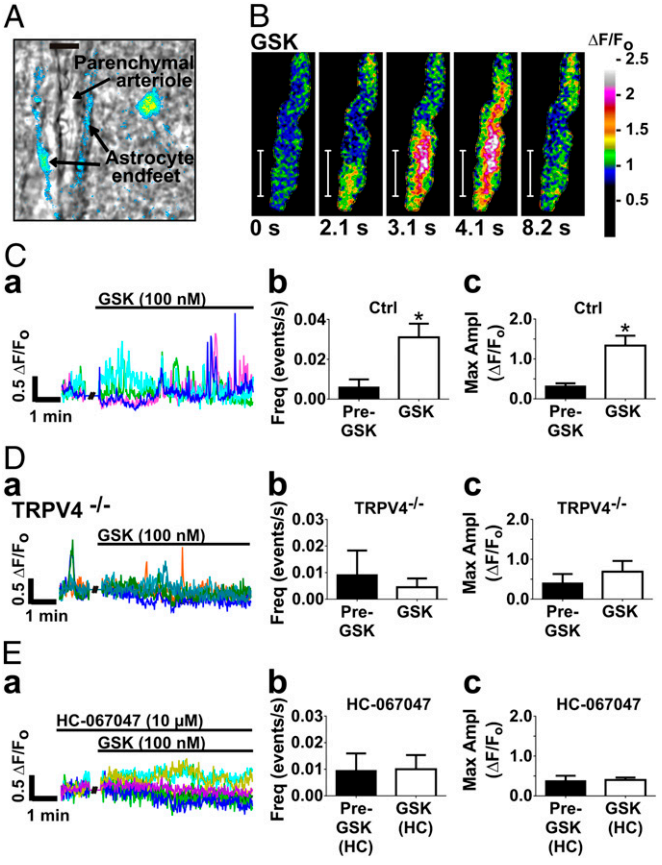

Fig. 1. Activation of TRPV4 with the agonist GSK1016790A (GSK) increases Ca^{2+} oscillations in astrocytic endfeet. (*A*) Pseudocolor Fluo-4 AM fluorescence representing $[Ca^{2+}]_i$ in astrocytic endfeet surrounding a parenchymal arteriole in a brain slice (field of view = 62 × 62 μm). (Scale bar, 10 μm.) In the image shown, Fluo-4 AM fluorescence can be observed in the astrocyte soma as well as the endfeet. (*B*) Time course of a propagating Ca^{2+} oscillation within an endfoot in response to GSK (100 nM). (Scale bar, 10 μm.) Total duration of the oscillation was 8.2 s. GSK stimulated fast, high-amplitude Ca^{2+} oscillations in astrocytic endfeet, mainly in the form of Ca^{2+} waves. (*C*, *a*; *D*, *a*; and *E*, *a*) Representative fractional fluorescence ($\Delta F/F_o$) traces from ROIs on perivascular astrocytic endfeet in one brain slice before and after addition of GSK. Each color represents one ROI. (*C*, *b* and *C*, *c*) GSK increased the frequency and maximum amplitude of endfoot Ca^{2+} oscillations ($P < 0.05$; n = 7 slices from six animals). (*D*) GSK had no effect in TRPV4$^{-/-}$ mice (n = 4 slices from two animals). (*E*, *b* and *E*, *c*) The effect of GSK on the frequency and amplitude of endfoot Ca^{2+} oscillations was blocked by the selective TRPV4 antagonist, HC-067047 (10 μM; n = 6 slices from from animals). Values were compared by paired t test.

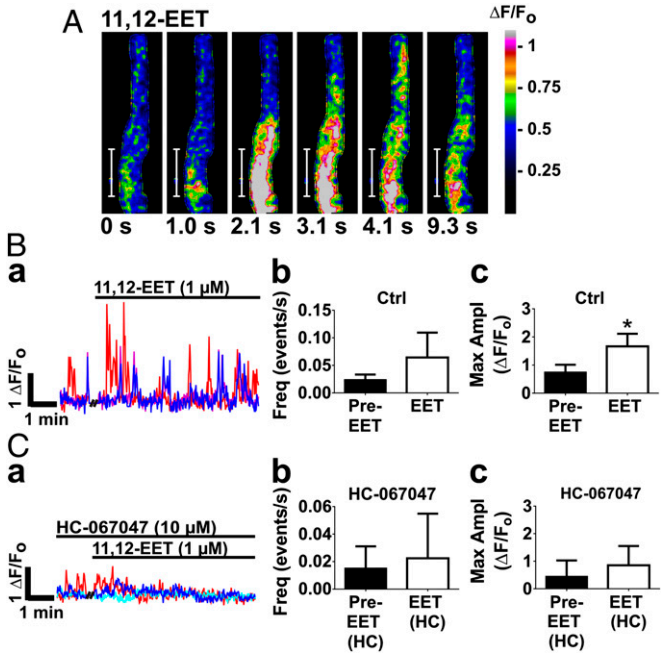

Fig. 2. The 11,12-EET increases endfoot Ca^{2+} oscillations via TRPV4 channels. (*A*) Time course of an 11,12-EET-stimulated Ca^{2+} oscillation in an astrocytic endfoot. (Scale bar, 10 μm.) The total duration of the oscillation was 9.3 s. (*B*, *a* and *B*, *c*) The 11,12-EET (1 μM) increased the amplitude of endfoot Ca^{2+} oscillations ($P < 0.05$; $n = 4$ slices from three animals), but did not significantly increase oscillation frequency (*B*, *b*). (*C*) Preincubation of brain slices with HC-067047 (1 μM) prevented the effect of 11,12-EET on endfoot Ca^{2+} oscillations ($n = 5$ slices from two animals). Values were compared by paired *t* test.

with CPA (Fig. 3*D*). The implication of these findings is that the long-duration, low-amplitude, spatially restricted Ca^{2+} oscillations elicited by GSK after depletion of ER Ca^{2+} reflect Ca^{2+} entry through TRPV4 channels. These results also suggest that, under normal conditions, Ca^{2+} entry through TRPV4 channels in astrocytic endfeet stimulates ER Ca^{2+} release, most likely by activating IP_3Rs, amplifying local Ca^{2+} increases and triggering Ca^{2+} waves. Although astrocytic endfeet lack functional ryanodine receptors and CPA prevents Ca^{2+} signals in response to IP_3 uncaging (6), we sought to validate the results obtained with CPA by using the IP_3R inhibitor, xestospongin C (XC). In agreement with previous reports (6), XC (20 μM) was only partially effective at inhibiting IP_3Rs in brain slices (Fig. S3*A*), reducing the IP_3R-mediated rise in endfoot Ca^{2+} to neuronal activation by electrical field stimulation (EFS) to 64% ± 11% of control ($n = 4$ slices from three animals) compared with 13% ± 4% with CPA ($n = 6$ slices from five animals). However, as was the case with CPA, in the presence of XC we observed slow, low-amplitude "TRPV4-like" endfoot Ca^{2+} events (Fig. S3*B*, *a*, purple trace) in response to GSK. GSK also elicited fast, high-amplitude "IP_3R-like" events (Fig. S3*B*, *a*, blue trace), consistent with only partial inhibition of IP_3Rs by XC. These results provide strong evidence that activation of TRPV4 channels in astrocytic endfeet stimulates IP_3R-mediated Ca^{2+} signaling.

Astrocytic Endfoot TRPV4 Channels Are Engaged in NVC and Augment the Endfoot Ca^{2+} Response to Neural Activation. Astrocytic endfoot $[Ca^{2+}]_i$ plays a central role in regulating local blood flow in the brain. Endfoot Ca^{2+} controls parenchymal arteriolar tone; thus, any mechanism that alters endfoot $[Ca^{2+}]_i$ has the potential to alter parenchymal arteriolar diameter. We previously reported a bimodal relationship between endfoot $[Ca^{2+}]_i$ and arteriolar diameter in which moderate increases in endfoot $[Ca^{2+}]_i$ elicit vasodilation, but high endfoot $[Ca^{2+}]_i$ produces vasoconstriction (10). Applying this observation to the current context, we found that in the presence of the TRPV4 agonist GSK (100 nM), the 10 highest amplitude TRPV4 Ca^{2+} oscillations (from six different animals) averaged 1.3 $\Delta F/F_o$, corresponding to an average increase in endfoot $[Ca^{2+}]_i$ of 154 ± 23 nM, and were associated with transient vasodilation of the parenchymal arteriole by 11% ± 3% (Fig. S4). Only one TRPV4 Ca^{2+} oscillation observed elicited a vascular response that trended toward constriction (~2%). These observations indicate that endfoot Ca^{2+} oscillations induced by TRPV4 activation influence parenchymal arteriolar tone but terminate before reaching endfoot $[Ca^{2+}]_i$ levels that produce vasoconstriction.

Given the importance of endfoot Ca^{2+} in NVC, we next sought to examine whether TRPV4 channels influence the rise in endfoot Ca^{2+} and the ensuing vasodilation during NVC. In brain slices, NVC was simulated by depolarizing neurons through EFS. Incubation with HC-067047 (10 μM) for 25 min decreased the EFS-evoked rise in endfoot $[Ca^{2+}]_i$ by 45% ± 8% (Fig. 4 *A* and *B*, *a*) and reduced the associated parenchymal arteriolar dilation from 19% ± 2–11% ± 2% ($n = 6$ slices from five animals) (Fig. 4 *A* and *B*, *b* and Movies S4 and S5). These effects were not observed in $TRPV4^{-/-}$ mice (Fig. S5) or in time-control experiments (Fig. S6). Notably, there was also a trend toward an attenuation in endfoot Ca^{2+} response to EFS in $TRPV4^{-/-}$ mice

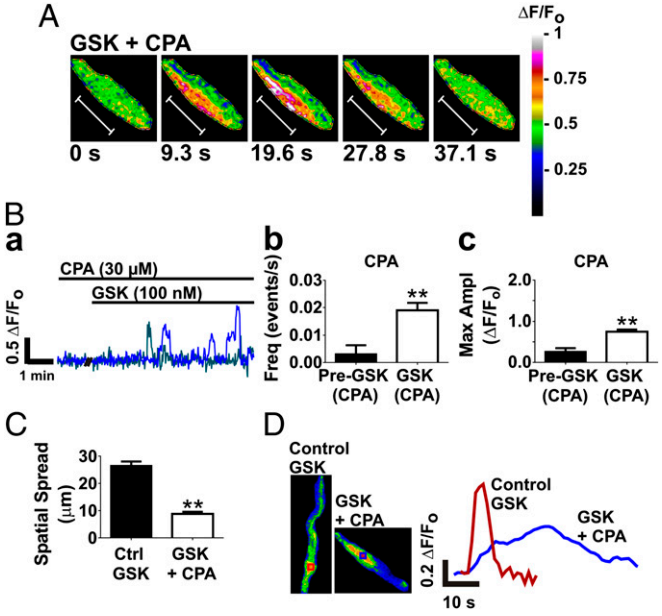

Fig. 3. TRPV4 Ca^{2+} entry in astrocytic endfeet stimulates IP_3R Ca^{2+} release, amplifying local Ca^{2+} increases and triggering Ca^{2+} waves. (*A*) Time course of a Ca^{2+} oscillation in response to GSK after depletion of ER Ca^{2+} stores with the SERCA pump inhibitor, CPA (30 μM). CPA eliminated Ca^{2+} waves in response to GSK. In the presence of CPA, GSK induced slow, low-amplitude Ca^{2+} oscillations. The total duration of the oscillation was 37.1 s. (Scale bar, 10 μm.) (*B*, *a*) A representative trace of fractional fluorescence changes within ROIs on astrocytic endfeet induced by stimulation with GSK in a brain slice preincubated with CPA. The frequency (*B*, *b*) and amplitude (*B*, *c*) of endfoot Ca^{2+} oscillations was still increased by stimulation with GSK in the presence of CPA ($P < 0.01$; $n = 6$ slices from four animals). (*C*) CPA reduced the average spatial spread of GSK-stimulated endfoot Ca^{2+} oscillations ($P < 0.001$; $n = 27$ for Control GSK; $n = 9$ for GSK + CPA). (*D*) Locally, Ca^{2+} increases to GSK were faster and of higher amplitude under normal conditions compared with when ER Ca^{2+} was depleted by CPA. Traces depict fluorescence in ROIs of corresponding color in image panels to the left. Values in *B* were compared by paired *t* test; values in *C* were compared by unpaired *t* test.

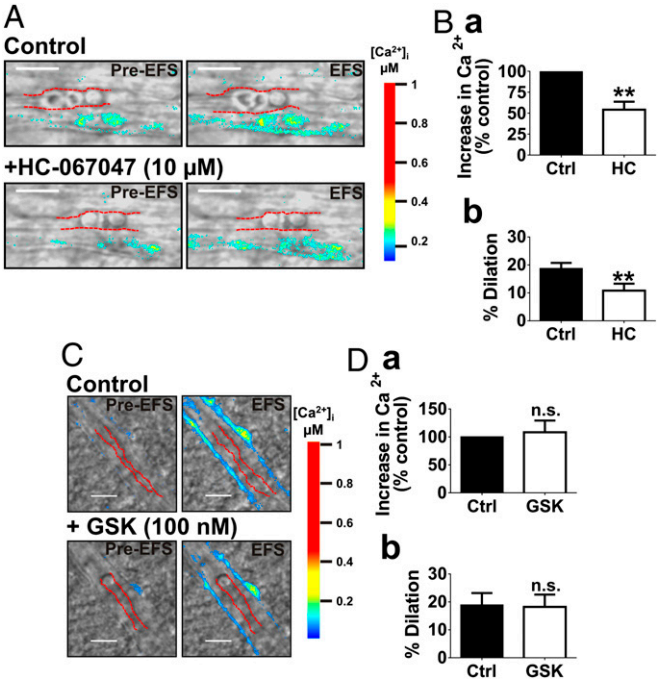

Fig. 4. Astrocytic TRPV4 channels contribute to NVC by augmenting the endfoot Ca^{2+} response to neuronal activation. (*A* and *C*) EFS-induced depolarization of neurons in brain slices caused a rise in endfoot Ca^{2+} and dilation of parenchymal arterioles under control conditions. (*A* and *B*) Preincubation of brain slices with the TRPV4 antagonist, HC-067047 (10 μM for 25 min), reduced the increase in endfoot $[Ca^{2+}]_i$ (*B*, *a*) and vasodilation (*B*, *b*) resulting from EFS ($P < 0.01$; $n = 6$ slices from five animals). (*C and D*) EFS-evoked increases in endfoot $[Ca^{2+}]_i$ (*D*, *a*) and vasodilation (*D*, *b*) were unchanged following a 10-min exposure to GSK (100 nM) ($n = 4$ slices from four animals). (Scale bar, 10 μm.) Values were compared by paired *t* test.

compared with WT ($P = 0.05$; $n = 4$ slices from three animals) (Fig. S5*B*, *a*). These findings suggest that endfoot TRPV4 channels contribute to the increase in endfoot $[Ca^{2+}]_i$ and vasodilation to neuronal activity, and thus are engaged during NVC.

Neither the rise in endfoot $[Ca^{2+}]_i$ ($n = 5$ slices from three animals) nor the vasodilation ($n = 4$ slices from four animals) evoked by EFS differed in the presence of GSK relative to controls (Fig. 4 *C* and *D*). Collectively, these observations suggest that while TRPV4 channels appear to be activated during NVC, contributing to the rise in endfoot $[Ca^{2+}]_i$ and augmenting the evoked dilation, there is a limit to their activation and the extent to which they can increase endfoot $[Ca^{2+}]_i$. This observation supports the concept that Ca^{2+} oscillations in astrocytic endfeet self-terminate, perhaps as a result of Ca^{2+}-dependent inhibition of Ca^{2+} entry and release channels.

Engagement of Astrocytic Endfoot TRPV4 Channels in NVC Is Not Mediated Through Activation by EETs. We have demonstrated here that exogenous 11,12-EET activates TRPV4 channels, increasing endfoot Ca^{2+} oscillations (Fig. 2). Therefore, the mechanism by which endfoot TRPV4 channels are activated during NVC may be through an autocrine effect of EETs, which are released by astrocytes in response to glutamate and are hypothesized to play a role in NVC (32, 33). To determine the role of EETs in TRPV4 channel activation during NVC, we examined endfoot Ca^{2+} and parenchymal arteriolar dilation responses to EFS after incubation with methyl arachidonyl fluorophosphonate (MAFP; 5 μM), an inhibitor of cytosolic and Ca^{2+}-independent forms of phospholipase A_2 (PLA_2) responsible for generating arachidonic acid, the precursor of EETs. Notably, incubation of brain slices with MAFP dilated parenchymal arterioles by 18% ± 4% ($n = 7$ slices from four animals) (Fig. 5*B*, *a*), suggesting a tonic contribution of arachidonic acid metabolites to resting arteriolar diameter in brain slices. MAFP also significantly attenuated parenchymal arteriolar dilation to EFS, decreasing vasodilation from 10% ± 1 to 7% ± 1% ($n = 7$ slices from four animals) (Fig. 5*B*, *c*). However, in contrast to HC-067047, MAFP did not affect EFS-evoked increases in endfoot $[Ca^{2+}]_i$ (Fig. 5*B*, *b*), indicating that the activation of TRPV4 channels during NVC is not mediated by EETs. The attenuation of EFS-evoked vasodilation by MAFP, considered in isolation, might be interpreted as evidence that EETs are astrocyte-derived mediators of vasodilation in NVC; however, because MAFP alone caused substantial dilation, this effect may simply reflect the diminished dilatory capacity of the arteriole.

TRPV4 Channels Contribute to NVC in Vivo. To test whether effects observed in the brain slice preparation translate to the intact animal, we examined the effect of TRPV4 inhibition on cerebral hemodynamic responses in vivo, using a cranial window model and laser Doppler flowmetry to measure local CBF in the somatosensory cortex of mice. Superfusion of the cortical brain surface for 25 min with HC-067047 (10 μM) had no effect on resting CBF ($n = 7$) (Fig. S7). NVC was assessed in vivo by recording the CBF response to contralateral whisker stimulation. HC-067047 attenuated the CBF response during 60 s whisker stimulation, calculated as total area under the curve, by 28% ± 6% ($n = 7$) (Fig. 6). These results provide further support for involvement of TRPV4 channels in NVC.

Discussion

Emerging evidence indicates that TRPV4 channels may play important roles in astrocyte function (12, 34). However, a characterization of TRPV4-mediated Ca^{2+} signals in astrocytes has been lacking. TRPV4 channel activity has also not been studied

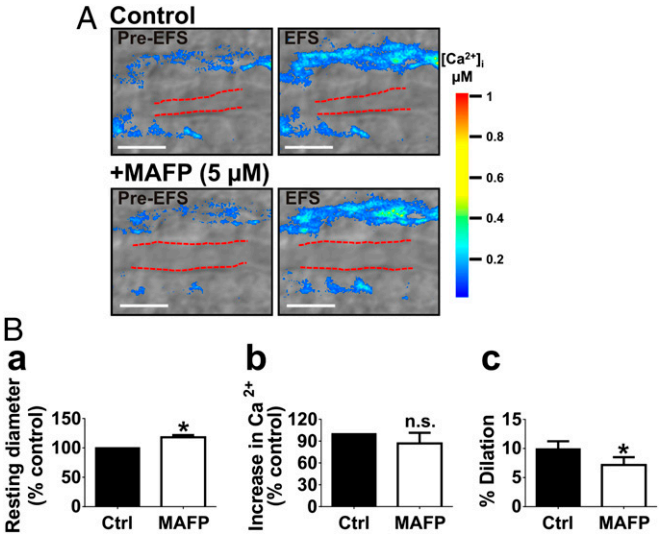

Fig. 5. Astrocytic endfoot TRPV4 channel activation during NVC is not mediated by EETs. Brain slices were incubated with MAFP (5 μM for 20 min), an inhibitor of cytosolic and Ca^{2+}-independent PLA_2, to block arachidonic acid production and the subsequent formation of cytochrome P450 (CYP) metabolites, including EETs. (*A*) Endfoot Ca^{2+} and parenchymal arteriole diameter responses to EFS before and after treatment with MAFP. (*B*, *a*) Incubation with MAFP dilated parenchymal arterioles before EFS ($P < 0.01$; $n = 7$ slices from four animals). In the presence of MAFP, the EFS-evoked increase in endfoot $[Ca^{2+}]_i$ did not differ from that in controls (*B*, *b*), but the evoked dilation was reduced (*B*, *c*) ($P < 0.01$; $n = 7$ slices from four animals). (Scale bar, 10 μm.) Values were compared by paired *t* test.

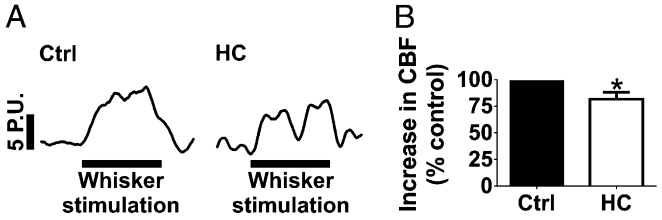

Fig. 6. TRPV4 channels contribute to NVC in vivo. (*A*) Representative CBF recordings, presented in laser Doppler perfusion units (P.U.s), from the somatosensory cortex during 60 s contralateral whisker stimulation (indicated by the black bar) before (*Left*) and after (*Right*) cortical superfusion of HC-067047 (10 μM). (*B*) Cortical superfusion of HC-067047 (10 μM) attenuated the increase in CBF to contralateral whisker stimulation ($P < 0.05$; $n = 7$). Values were compared by paired *t* test.

in astrocytic microdomains, such as the perivascular endfoot, in which Ca^{2+} signaling has a profound impact on the local microcirculation. The aims of this study were to characterize TRPV4-mediated Ca^{2+} signaling in perivascular endfeet of cortical astrocytes in situ and explore the contribution of TRPV4 channels to astrocytic regulation of the cerebral microcirculation.

Our results provide evidence of functional TRPV4 channels in astrocytic endfeet and suggest a dynamic interplay between endfoot TRPV4 channels and IP_3Rs that likely reflects the bimodal Ca^{2+} dependence of both channel types. We found that GSK and 11,12-EET stimulated TRPV4 channel-dependent Ca^{2+} oscillations in cortical astrocytic endfeet, and these oscillations exhibited fast kinetics, were high amplitude, and were largely in the form of propagating Ca^{2+} waves (Figs. 1 and 2). Minimizing IP_3R-mediated Ca^{2+} release by ER Ca^{2+} store depletion or IP_3R inhibition transformed GSK-induced Ca^{2+} oscillations from fast, high-amplitude, propagating events to slow, low-amplitude, localized events, providing evidence that direct activation of TRPV4 channels increases IP_3R-dependent Ca^{2+} signaling (Fig. 3 and Fig. S3). The implication is that Ca^{2+} entry through TRPV4 channels triggers the activation of IP_3Rs, amplifying local Ca^{2+} signals and initiating Ca^{2+} waves. The rapid termination of these oscillations may reflect inhibition of IP_3Rs and TRPV4 channels by high-amplitude increases in local $[Ca^{2+}]_i$. Conversely, the prolonged duration of TRPV4 Ca^{2+} signals observed when IP_3R activity is eliminated may be explained by delayed Ca^{2+}-dependent inhibition of TRPV4 channels as a result of the lower amplitude of these oscillations. The ability of TRPV4 channel-mediated Ca^{2+} signals to be amplified and transmitted to distant locations within the endfoot and/or throughout the astrocyte via the generation of IP_3R-dependent Ca^{2+} waves is significant in that it provides a potential mechanism by which signals arising from the vasculature may be sensed by the endfoot and communicated "upstream" to other regions of the astrocyte, as well as to neurons and interneurons.

Spontaneous Ca^{2+} oscillations occurring in astrocytes at rest are dependent on IP_3Rs (Fig. S2*B*) (35, 36). Based on our observation that TRPV4 channel activation triggered IP_3R-mediated Ca^{2+} oscillations, we had originally hypothesized that spontaneous astrocytic Ca^{2+} oscillations are triggered by Ca^{2+} influx through TRPV4 channels. However, a lack of effect of the TRPV4 channel antagonist and persistence of these events in TRPV4$^{-/-}$ mice indicate that basal TRPV4 channel activity does not drive spontaneous endfoot Ca^{2+} oscillations.

Endfoot-restricted increases in $[Ca^{2+}]_i$ produced by flash photolysis of caged IP_3/Ca^{2+} change parenchymal arteriolar diameter, demonstrating that endfoot Ca^{2+} signals control arteriolar tone and local perfusion (6, 10, 37). Excessive elevations of endfoot Ca^{2+} can induce vasoconstriction (10). We found that the 10 highest amplitude endfoot Ca^{2+} oscillations observed with TRPV4 channel activation transiently dilated parenchymal arterioles by an average of 11%. The highest amplitude oscillation observed appeared to be at the threshold of endfoot $[Ca^{2+}]_i$ at which the vascular response switches from dilation to constriction. These results suggest that increases in endfoot $[Ca^{2+}]_i$ initiated by astrocytic TRPV4 channels can cause vasodilation and, secondly, that these Ca^{2+} oscillations terminate before reaching a $[Ca^{2+}]_i$ that might elicit vasoconstriction. A likely explanation for this phenomenon lies in the biphasic Ca^{2+}-dependent modulation of IP_3R and TRPV4 gating, in which Ca^{2+} activates these channels at lower concentrations and inhibits at higher concentrations (25–29). Therefore, astrocytic TRPV4 channel activation is not associated with vasoconstriction in the brain—a characteristic that underscores the potential physiological relevance of this signaling pathway in astrocyte function.

There has been very little evidence that extracellular Ca^{2+} entry contributes to Ca^{2+} signaling in astrocytes during NVC. We found that inhibition of TRPV4 channels with HC-067047 reduced the neuronally evoked elevation of endfoot $[Ca^{2+}]_i$ and vasodilation by about 45% in brain slices. The effect of TRPV4 channel inhibition on NVC in brain slices was supported in vivo by a 28% reduction in the CBF response to whisker stimulation. These results indicate that astrocytic TRPV4 channels contribute to vasodilation in NVC by augmenting the endfoot $[Ca^{2+}]_i$ rise in response to neuronal activity.

Two potential mechanisms that might engage astrocytic TRPV4 channels during NVC are activation of TRPV4 channels by Ca^{2+} released into the cytosol through IP_3Rs, or an autocrine effect of EETs, which can be released by astrocytes during NVC (32). We found that the endfoot Ca^{2+} response to EFS was not diminished in the presence of the PLA_2 inhibitor, MAFP, which prevents the formation of arachidonic acid, the substrate for EETs synthesis. Thus, EETs are not likely involved in activating TRPV4 channels during NVC. This observation further supports a bidirectional synergy between IP_3Rs and TRPV4 channels, pointing to Ca^{2+} as a possible mediator of TRPV4 channel activation in astrocytes during NVC. Although MAFP had no effect on the endfoot Ca^{2+} response, it did reduce the dilation to EFS. However, whether the attenuation of EFS-evoked arteriolar vasodilation by MAFP is due to inhibition of EETs synthesis or is simply secondary to its dilatory effect on resting diameter cannot be concluded from these results. The effect of MAFP on resting diameter is itself noteworthy, as it suggests a tonic contribution of a vasoconstrictor metabolite of arachidonic acid, such as 20-hydroxyeicosatetraenoic acid (20-HETE) or prostaglandin E_2 (PGE_2), to parenchymal arteriolar tone (38, 39).

Based on evidence obtained by direct activation of TRPV4 channels and activation of IP_3Rs by neuronal activity, we propose a model in which activation of either channel reciprocally stimulates opening of the other channel through activation by Ca^{2+}. According to this model, neuronal stimulation causes an elevation of astrocytic IP_3, leading to an elevation of endfoot Ca^{2+} that, in turn, activates TRPV4 channels. In addition, under circumstances in which astrocytic endfoot TRPV4 channels are activated, Ca^{2+} entry activates IP_3Rs, amplifying local Ca^{2+} signals and stimulating neighboring IP_3Rs to produce Ca^{2+} waves. These Ca^{2+} signals ultimately terminate through Ca^{2+}-dependent inhibition of both IP_3Rs and TRPV4 channels. Together these observations suggest a bidirectional, reciprocal interaction between TRPV4 channels and IP_3Rs, and confirm that TRPV4 channels play a dynamic role in sculpting Ca^{2+} signaling in the endfoot microdomain and therefore contribute to astrocyte-mediated regulation of the cerebral microcirculation. Moreover, we propose that amplification and conduction of TRPV4-initiated Ca^{2+} signals by IP_3Rs may be an important mechanism by which endfeet sense signals arising from the vasculature to modulate astrocytic function and, by extension, neuronal function.

Materials and Methods

Animal Procedures. Experiments were performed using 2–3-mo-old male C57BL/6 (Jackson Laboratories) and TRPV4$^{-/-}$ (40) mice. All animal procedures were approved by the Office of Animal Care Management at the University of Vermont and were performed in accordance with the *Guide for the Care and Use of Laboratory Animals* of the National Institutes of Health.

Multiphoton Imaging of Astrocytic Endfoot Ca^{2+} and Parenchymal Arteriole Diameter in Brain Slices. Cortical astrocytic endfoot Ca^{2+} dynamics and parenchymal arteriole diameter were imaged in coronal brain slices as previously described (10). Brains from mice overdosed with sodium pentobarbital were rapidly removed and placed in ice-cold artificial cerebral spinal fluid (aCSF; for composition, see *SI Materials and Methods*). Coronal brain slices were cut with a vibratome (VT1000S; Leica Microsystems Inc.) to 160-μm thickness. Slices were stored at room temperature in aCSF (20–25 °C) continuously bubbled with 95% O_2/5% CO_2 before dye loading.

Slices were loaded with the Ca^{2+} indicator dye, Fluo-4 AM (10 μM), and 2.5 mg/mL pluronic acid for 90–100 min at 29 °C. Under these loading conditions, the dye is preferentially taken up by astrocytes. Slices were rinsed of the dye solution following the incubation period and kept in aCSF until imaged. For imaging, individual slices were transferred to a perfusion chamber and continuously perfused with aCSF equilibrated with 95% O_2/5% CO_2 containing the thromboxane A2 receptor agonist 9,11-dideoxy-11α,9α-epoxymethanoprostaglandin F2α (U-46619; 125 nM) and maintained at 35 °C. U-46619 was added to the perfusate to preconstrict arterioles in the brain slice to simulate basal arterial tone in vivo, as we have done previously (5, 6, 8, 10). Parenchymal arterioles in the region of the somatosensory cortex were chosen for imaging. Astrocytic endfoot Ca^{2+} and diameter of adjacent arterioles were simultaneously imaged using two-photon laser-scanning microscopy (BioRad Radiance 2100MP) and IR-DIC microscopy, respectively. The two-photon microscope was coupled to a Chameleon Ti: sapphire laser (141-fs pulses, 1.5 W; Coherent, Inc.) and an upright microscope with a 20× water-dipping objective (Olympus XLUMPlan FI BX51WI; 0.95 N. A.; Olympus America). Images were acquired using BioRad Laser-Sharp 2000 software. Fluo-4 AM was excited at 820 nm, and emission was collected using a 575/150-nm band-pass filter.

For detailed information on imaging analysis, EFS in brain slices, in vivo CBF measurement, and reagents, please refer to *SI Materials and Methods*. All values are expressed as means ± SEMs.

ACKNOWLEDGMENTS. We thank Dr. Adrian Bonev for technical advice. This work was supported by grants from the National Institutes of Health (P01 HL095488, R01 HL44455, R01 HL098243, T32 HL07944, R37 DK053832, and 8P30GM103498-02), the Fondation Leducq for the Transatlantic Network of Excellence on the Pathogenesis of Small Vessel Disease of the Brain, and the Totman Medical Research Trust.

1. Halassa MM, Fellin T, Takano H, Dong JH, Haydon PG (2007) Synaptic islands defined by the territory of a single astrocyte. *J Neurosci* 27(24):6473–6477.
2. Simard M, Arcuino G, Takano T, Liu QS, Nedergaard M (2003) Signaling at the gliovascular interface. *J Neurosci* 23(27):9254–9262.
3. Parpura V, et al. (1994) Glutamate-mediated astrocyte-neuron signalling. *Nature* 369(6483):744–747.
4. Pryazhnikov E, Khiroug L (2008) Sub-micromolar increase in [Ca(2+)](i) triggers delayed exocytosis of ATP in cultured astrocytes. *Glia* 56(1):38–49.
5. Filosa JA, Bonev AD, Nelson MT (2004) Calcium dynamics in cortical astrocytes and arterioles during neurovascular coupling. *Circ Res* 95(10):e73–e81.
6. Straub SV, Bonev AD, Wilkerson MK, Nelson MT (2006) Dynamic inositol trisphosphate-mediated calcium signals within astrocytic endfeet underlie vasodilation of cerebral arterioles. *J Gen Physiol* 128(6):659–669.
7. Zonta M, et al. (2003) Neuron-to-astrocyte signaling is central to the dynamic control of brain microcirculation. *Nat Neurosci* 6(1):43–50.
8. Filosa JA, et al. (2006) Local potassium signaling couples neuronal activity to vasodilation in the brain. *Nat Neurosci* 9(11):1397–1403.
9. Straub SV, Nelson MT (2007) Astrocytic calcium signaling: The information currency coupling neuronal activity to the cerebral microcirculation. *Trends Cardiovasc Med* 17(6):183–190.
10. Girouard H, et al. (2010) Astrocytic endfoot Ca2+ and BK channels determine both arteriolar dilation and constriction. *Proc Natl Acad Sci USA* 107(8):3811–3816.
11. Benfenati V, et al. (2007) Expression and functional characterization of transient receptor potential vanilloid-related channel 4 (TRPV4) in rat cortical astrocytes. *Neuroscience* 148(4):876–892.
12. Benfenati V, et al. (2011) An aquaporin-4/transient receptor potential vanilloid 4 (AQP4/TRPV4) complex is essential for cell-volume control in astrocytes. *Proc Natl Acad Sci USA* 108(6):2563–2568.
13. Watanabe H, et al. (2003) Anandamide and arachidonic acid use epoxyeicosatrienoic acids to activate TRPV4 channels. *Nature* 424(6947):434–438.
14. Fang X, Weintraub NL, Stoll LL, Spector AA (1999) Epoxyeicosatrienoic acids increase intracellular calcium concentration in vascular smooth muscle cells. *Hypertension* 34(6):1242–1246.
15. Earley S, Heppner TJ, Nelson MT, Brayden JE (2005) TRPV4 forms a novel Ca2+ signaling complex with ryanodine receptors and BKCa channels. *Circ Res* 97(12): 1270–1279.
16. Metea MR, Newman EA (2006) Glial cells dilate and constrict blood vessels: A mechanism of neurovascular coupling. *J Neurosci* 26(11):2862–2870.
17. Shi Y, et al. (2008) Interaction of mechanisms involving epoxyeicosatrienoic acids, adenosine receptors, and metabotropic glutamate receptors in neurovascular coupling in rat whisker barrel cortex. *J Cereb Blood Flow Metab* 28(1):111–125.
18. Lecrux C, Kocharyan A, Sandoe CH, Tong XK, Hamel E (2012) Pyramidal cells and cytochrome P450 epoxygenase products in the neurovascular coupling response to basal forebrain cholinergic input. *J Cereb Blood Flow Metab* 32(5):896–906.
19. Rzigalinski BA, Willoughby KA, Hoffman SW, Falck JR, Ellis EF (1999) Calcium influx factor, further evidence it is 5, 6-epoxyeicosatrienoic acid. *J Biol Chem* 274(1):175–182.
20. Higashimori H, Blanco VM, Tuniki VR, Falck JR, Filosa JA (2010) Role of epoxyeicosatrienoic acids as autocrine metabolites in glutamate-mediated K+ signaling in perivascular astrocytes. *Am J Physiol Cell Physiol* 299(5):C1068–C1078.
21. Vriens J, et al. (2004) Cell swelling, heat, and chemical agonists use distinct pathways for the activation of the cation channel TRPV4. *Proc Natl Acad Sci USA* 101(1): 396–401.
22. Güler AD, et al. (2002) Heat-evoked activation of the ion channel, TRPV4. *J Neurosci* 22(15):6408–6414.
23. Nilius B, Owsianik G, Voets T, Peters JA (2007) Transient receptor potential cation channels in disease. *Physiol Rev* 87(1):165–217.
24. Nilius B, Watanabe H, Vriens J (2003) The TRPV4 channel: Structure-function relationship and promiscuous gating behaviour. *Pflugers Arch* 446(3):298–303.
25. Strotmann R, Schultz G, Plant TD (2003) Ca2+-dependent potentiation of the nonselective cation channel TRPV4 is mediated by a C-terminal calmodulin binding site. *J Biol Chem* 278(29):26541–26549.
26. Watanabe H, et al. (2003) Modulation of TRPV4 gating by intra- and extracellular Ca2+. *Cell Calcium* 33(5-6):489–495.
27. Foskett JK, White C, Cheung KH, Mak DO (2007) Inositol trisphosphate receptor Ca2+ release channels. *Physiol Rev* 87(2):593–658.
28. Mak DO, McBride SM, Petrenko NB, Foskett JK (2003) Novel regulation of calcium inhibition of the inositol 1,4,5-trisphosphate receptor calcium-release channel. *J Gen Physiol* 122(5):569–581.
29. Kaftan EJ, Ehrlich BE, Watras J (1997) Inositol 1,4,5-trisphosphate (InsP3) and calcium interact to increase the dynamic range of InsP3 receptor-dependent calcium signaling. *J Gen Physiol* 110(5):529–538.
30. Thorneloe KS, et al. (2008) N-((1S)-1-[4-((2S)-2-[(2,4-dichlorophenyl)sulfonyl]amino-3-hydroxypropanoyl)-1-piperazinyl]carbonyl-3-methylbutyl)-1-benzothiophene-2-carboxamide (GSK1016790A), a novel and potent transient receptor potential vanilloid 4 channel agonist induces urinary bladder contraction and hyperactivity: Part I. *J Pharmacol Exp Ther* 326(2):432–442.
31. Everaerts W, et al. (2010) Inhibition of the cation channel TRPV4 improves bladder function in mice and rats with cyclophosphamide-induced cystitis. *Proc Natl Acad Sci USA* 107(44):19084–19089.
32. Alkayed NJ, et al. (1997) Role of P-450 arachidonic acid epoxygenase in the response of cerebral blood flow to glutamate in rats. *Stroke* 28(5):1066–1072.
33. Harder DR, Alkayed NJ, Lange AR, Gebremedhin D, Roman RJ (1998) Functional hyperemia in the brain: Hypothesis for astrocyte-derived vasodilator metabolites. *Stroke* 29(1):229–234.
34. Butenko O, et al. (2012) The increased activity of TRPV4 channel in the astrocytes of the adult rat hippocampus after cerebral hypoxia/ischemia. *PLoS ONE* 7(6):e39959.
35. Parri HR, Crunelli V (2003) The role of Ca2+ in the generation of spontaneous astrocytic Ca2+ oscillations. *Neuroscience* 120(4):979–992.
36. Nett WJ, Oloff SH, McCarthy KD (2002) Hippocampal astrocytes in situ exhibit calcium oscillations that occur independent of neuronal activity. *J Neurophysiol* 87(1): 528–537.
37. Takano T, et al. (2006) Astrocyte-mediated control of cerebral blood flow. *Nat Neurosci* 9(2):260–267.
38. Yu M, et al. (2004) Effects of a 20-HETE antagonist and agonists on cerebral vascular tone. *Eur J Pharmacol* 486(3):297–306.
39. Dabertrand F, et al. (2013) Prostaglandin E(2), a postulated astrocyte-derived neurovascular coupling agent, constricts rather than dilates parenchymal arterioles. *J Cereb Blood Flow Metab*.
40. Liedtke W, Friedman JM (2003) Abnormal osmotic regulation in trpv4-/- mice. *Proc Natl Acad Sci USA* 100(23):13698–13703.